Journal of Applied Fluid Mechanics, Vol. 13, No. 1, pp. 1-13, 2020.
Available online at www.jafmonline.net, ISSN 1735-3572, EISSN 1735-3645.
DOI: 10.29252/jafm.13.01.30075

Heat Conduction Characteristic of Rarefied Gas in Nanochannel

R. Rabani[1], G. Heidarinejad[1†], J. Harting[2, 3] and E. Shirani[4]

[1] *Faculty of Mechanical Engineering, Tarbiat Modares University, Tehran, 14115143, Iran*
[2] *Helmholtz Institute Erlangen-Nürnberg for Renewable Energy (IEK-11), Forschungszentrum Jülich, Fürther Strasse 248, Nuremberg, 90429, Germany*
[3] *Department of Applied Physics, Eindhoven University of Technology, 5600MB Eindhoven, PO box 513, The Netherlands*
[4] *Department of Mechanical Engineering, Foolad Institute of Technology, Fooladshahr, Isfahan, 8491663763, Iran*

†*Corresponding Author Email: gheidari@modares.ac.ir*

(Received January 24, 2019; accepted May 22, 2019)

ABSTRACT

Nonequilibrium molecular dynamics simulations is applied to investigate the simultaneous effect of rarefaction and wall force field on the heat conduction characteristics of nano-confined rarefied argon gas. The interactive thermal wall model is used to specify the desired temperature on the walls while the Irving–Kirkwood expression is implemented for calculating the heat flux. It is observed that as the temperature differences between the walls increases by lowering the temperature of the cold wall, the number of adsorbed gas atoms on the cold wall increases notably due to the increment in the residence time of the gas atoms. Consequently, the interfacial thermal resistance between the gas and the cold wall reduces which results in a reduction of the temperature jump. Meanwhile, the increase in the temperature of the hot wall leads to a reduction of the residence time of gas atoms in the near-wall region which decreases the number of absorbed gas atoms on the hot wall. This results in an increase in interfacial thermal resistance which leads to a higher temperature jump. It is observed that the bulk, wall force field and interface regions form approximately 10%, 45% and 45% of the total thermal resistance, respectively. Furthermore, unlike the interfacial thermal resistance, the bulk and the wall force field thermal resistance are approximately independent of the implemented temperature difference.

Keywords: Thermal resistance; Temperature jump; Gas atoms distribution; Molecular dynamics.

NOMENCLATURE

e_i	sum of kinetic and potential energy for *ith* molecule
f_{ij}	two-body force between i and j
H	channel height
h	microscopic enthalpy
J	microscopic heat flux vector
k	modified Knudsen number
k_b	Boltzmann constant
K_{eff}	effective thermal conductivity
Kn	Knudsen number
K_S	spring constant
L	channel length
m	molecule mass
n_{avr}	number of time steps in averaging stage
n_{ssc}	number of time steps to reach steady state condition
r	molecule position vector
r_c	cut-off radius
r_{ij}	interatomic distance between i and j
t	time
T	temperature
T_C	cold wall temperature
T_H	hot wall temperature
$T_{gas,Max}$	maximum temperature of the gas
$T_{gas,Min}$	minimum temperature of the gas
ϕ	intermolecular potential
v_i	velocity of molecule i
W	channel width
x, y, z	axial coordinates

ε	depth of the potential well
λ	mean free path
ρ	density
σ	molecular diameter

Subscript

g	gas
gg	gas-gas
i, j	counter
w	wall
wg	wall-gas

Abbreviations

MD	Molecular Dynamics
SWMD	Smart Wall Molecular Dynamics
ITWM	Interactive Thermal Wal l Model

1. INTRODUCTION

With significant improvement in the fabrication of nanoscale devices over the past decades, the scale of electronic devices continuously decreases toward nanometer sizes which leads to a notable increase in the power density (Pop, 2010). Besides, in order to avoid thermal failure and to increase the lifetime of such devices, the waste heat which is considerable at this high generation rate should be dissipated efficiently. Due to the smaller spatial and temporal scale, the large surface to volume ratio and the presence of the surface force field, heat transfer at the nanoscale is remarkably different from the conventional flow (Morciano *et al.*, 2017; Rebay, Kabar, & Kakaç, 2016; Soong, Yen, & Tzeng, 2007; Volz & Carminati, 2007). The non-equilibrium transport effect at such scales is classified based on the Knudsen number ($Kn=\lambda/H$), which is the ratio of the gas mean free path (λ) to the characteristic length-scale of the domain (H). According to the Knudsen number, molecular transport is considered as the continuum $Kn\leq0.01$, slip $0.01\leq Kn\leq0.1$, transition $0.1\leq Kn\leq10$ and free molecular $Kn\geq10$ regimes (Schaaf and Chambr, 1961). While at such scale, the non-equilibrium effect through the gas can be analyzed by the use of kinetic theory, the wall force field and surface adsorption should be treated by MD simulations since kinetic theory neglect the effects of the nano-confinement (Barisik & Beskok, 2014). It was observed that an exact MD simulation of rarefied gas flows requires computational domains that are at least one mean free path long in the periodic directions. This leads to an excessive number of wall molecules. Furthermore, MD simulations of the gas have to be performed for several intermolecular collision times to be able to have a reasonable approximation of macroscopic quantities from the molecular level information through averaging (Barisik, Kim, & Beskok, 2010).

Due to the reasons mentioned above, studies on the heat transfer characteristics of nanoconfined gas media are limited to dense gases or gases in the early transition regime where a small system length in the periodic directions is sufficient. The gas density, temperature and velocity profiles for dense gases, 400 kg/m$^3\leq\rho\leq$1000 kg/m^3, is studied and it was observed that increasing the wall-gas interaction strength leads to an increase in conductivity of solid to stationary gas and decreases the flow velocity near the interface (Markvoort, Hilbers, & Nedea, 2005). Furthermore, thermophysical properties of argon gas flow between parallel platinum walls at various rarefaction levels in the early transition regime (Kn=0.1~0.526) were studied while the channel walls were maintained at a constant temperature. In this study, the gravity-driven Poiseuille flow properties such as collision frequency on the walls, velocity and density profiles across the channel height were investigated, and it was shown that the value of tangential momentum accommodation coefficient had been decreased as the Knudsen and the gravity were increased (Prabha & Sathian, 2013). In order to reduce the computational time, the smart wall molecular dynamics (SWMD) algorithm is proposed (Barisik *et al.*, 2010). It was observed that the solution domain in the periodic direction should extend at least one mean free path. Based on the SWMD method which is considered as a cold wall model, systematic studies of the rarefied gas transport mechanism were performed and it was shown that interactions between wall and gas molecules determine flow physics in the bulk flow and near wall regions (Barisik & Beskok, 2011a, 2011b, 2012, 2014, 2016; Barisik *et al.*, 2010). Besides the gas-gas interaction, it was observed that solid surfaces induce forces on the gas molecules which penetrate up to approximately three molecular diameters (~1 nm) from each wall into the gas medium. Indeed, for a 5 nm channel, approximately 40% of the gas domain is affected by the wall force field which is a considerable portion. The transport phenomena in this region deviate significantly from the bulk region. It is shown that in this region the gas density (Barisik & Beskok, 2011a, 2011b; Kammara, Malaikannan, & Kumar, 2016; Yasuoka, Kaneda, & Suga, 2016), velocity (Barisik & Beskok, 2011b, 2012, 2014, 2016; Kammara *et al.*, 2016; Yasuoka *et al.*, 2016), shear and normal stress (Barisik & Beskok, 2011a) are entirely different from what is observed in the bulk region.

Recently, another cold wall model which is called "virtual-wall model" was proposed to describe fluid-wall molecular interactions, in order to reduce the computational time further (Qian, Tu, Bao, & Zhang, 2016). The wall force, which was acting on a fluid molecule, was calculated based on the fluid molecules distance from the wall and it was stored. Therefore, there is no need to calculate the fluid-wall interaction for each fluid molecules separately that leads to a considerable

reduction of computational time. The model was applied to the Couette and Poiseuille flows while a great agreement with the atomistic wall was observed.

The preceding review reveals that several aspects of the effect of the wall force field on the hydrodynamic behavior of gas within nanochannels are studied comprehensively by the use of SWMD and the virtual-wall model. It should be noticed that due to the cold wall nature of this method, the heat transfer characteristics of the gas medium could not be studied. As an example in all previous studies, the excess heat that is generated due to the collision between the moving walls and the gas molecules is removed through the thermostat that is applied to the gas medium. Besides, the temperature differences between the channel walls and the gas medium lead to a notable heat transport through the system in several applications. This heat transfer should be considered in the simulations and cannot be neglected (Liu *et al.*, 2007; Matthes, Knigge, & Talke, 2014; Myo, Zhou, Yu, & Hua, 2011; Zhou, Liu, Yu, & Hua, 2010; Zhou, Yu, Hua, & Myo, 2013). Unlike the gas, it should be noted that the heat transfer characteristics through the liquid medium have been studied extensively by implementation of thermal wall on the channel (Amani, Karimian, & Seyednia, 2017; Cao, Sun, Chen, & Guo, 2009; Faraji & Rajabpour, 2017; Fu & Wang, 2018; Ge, Gu, & Chen, 2015; Ghorbanian & Beskok, 2017; Jepps, Bhatia, & Searles, 2004; Wang, Cheng, & Quan, 2016).

The objective of this manuscript is to investigate the heat transfer characteristics of a rarefied gas medium confined in a nanochannel. We investigate the heat conduction through the gas confined between two parallel plates of the distance H=5.4 nm. The gas density is considered as ρ=1.896 Kg/m^3 which leads to modified Knudsen number of k=10 (Barisik & Beskok, 2011a, 2011b). Under such conditions, simultaneous effects of the gas rarefaction, surface adsorption and wall force field on the heat transfer characteristics through the gas medium can be observed. It was shown that the timestep of 4 fs is adequate to resolve momentum transfer through the nanoconfined gas medium (Barisik *et al.*, 2010). In order to investigate whether 4 fs is adequate to resolve the heat transfer in the rarefied gas domain, smaller timesteps have been tested initially. Then the validation of the solution is investigated by comparison between the current solution and the previously published result (Barisik & Beskok, 2011b). Due to the substantial number of wall molecules which arise from extending the domain boundary in the periodic direction, the gas density and temperature of 2-D and 3-D domains for the same solution parameter are compared to see whether the 2-D solution is accurate enough for simulations. Finally, the temperature difference between the walls has been changed in order to observe its effect on the thermal transport characteristics of the gas medium such as the normalized temperature profile, the density distributions, the thermal conductivity and the thermal resistance of the gas medium.

2. THREE-DIMENSIONAL MD DETAILS

Heat conduction through the argon gas between two parallel plates is simulated by implementing the MD code LAMMPS (Large-Scale Atomic/Molecular Massively Parallel Simulator) from Sandia National Laboratories (Plimpton, 1995). A truncated (6–12) Lennard–Jones (L–J) potential, which is used to model the van der Waals interactions between different types of molecules, is given as follows:

$$\phi_{(r_{ij})} = \begin{cases} 4\varepsilon\left[\left(\frac{\sigma}{r_{ij}}\right)^{12} - \left(\frac{\sigma}{r_{ij}}\right)^{6}\right] - \varnothing(r_C) & r \le r_C \\ 0 & r > r_C \end{cases} \quad (1)$$

As the system potential is determined, the equations of motion for the particle *i* are given by:

$$m\frac{d^2r}{dt^2} = -\sum_{i\neq j}\nabla\varphi_{ij}^{T} \quad (2)$$

where ε is depth of the potential well, σ is molecular diameter, m is molecule mass, r_{ij} is interatomic distance between molecules i and j, r_c is the cut-off radius and the r is molecule position vector. In order to find the position and velocity of molecules at each time step, the velocity Verlet algorithm is used for time integration (Allen, Tildesley, & Banavar, 1989).

One of the most efficient methods in controlling the temperature of the walls is the interactive thermal wall model (ITWM) in which bond spring are attached to the walls molecules at their lattice positions (Kim, Beskok, & Cagin, 2008). In order to implement the thermal interaction between the wall and fluid molecules in this method properly, the fluid molecules forces on the wall molecules motion should be considered in to account while the interaction between the walls molecules is reduced to a crystal bond stiffness and each of them is regarded as an independent oscillator. Furthermore, to specify the desired temperature on the walls, a velocity-scaling thermostat is applied to each layer of the wall separately which result in a uniform temperature on the wall. The value of K_S=500εσ^{-2} is considered as the wall stiffness (K_S) which determines the strength of the bonds between the wall particles (Asproulis & Drikakis, 2010).

The physical properties of the argon gas are considered as m_g=6.63×10^{-26} Kg, σ_g=0.3405 nm, r_c=1.08 nm and ε_{gg}=119.8×k_b where k_b=1.3806×10^{-23} J/K (Barisik & Beskok, 2011a, 2014, 2015, 2016). For the walls, the same molecular mass and diameter are considered for the walls molecules. Furthermore, it was assumed that the potential strength for gas-wall interactions is equal to potential strength for gas-gas interaction (Barisik & Beskok, 2011a, 2011b, 2016) which mean that m_w= m_g, σ_w= σ_g and σ_w= σ_g. Figure 1 shows a schematic representation of the wall molecules. In this study,

two layers of FCC structure is used to model the wall due to the cut off radius which is considered and this is in complete accordance with the previous studies (Barisik & Beskok, 2011a, 2011b, 2014, 2016). All simulations are started from the Maxwell–Boltzmann velocity distribution for argon and wall molecules with NVE ensemble at the initial temperature of 298 K.

We let the initial particle distribution to evolve for 10^6 time steps to reach thermal equilibrium after which heat is induced into the domain by applying T_H and T_C to upper and bottom wall respectively and n_{ssc} time steps is done to attain steady state condition with the new heat flux conditions. Additionally, in order to average the microscopic quantity to attain macroscopic properties, n_{avr} time steps are performed. It should be considered that in order to confirm convergence of macroscopic quantity, longer time averaging is also performed in each case.

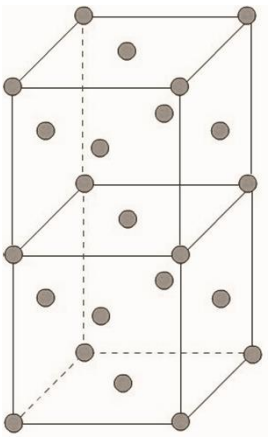

Fig. 1. Schematic sketch of two adjacent FCC structure of the wall.

The exact values for n_{ssc}, n_{avr}, T_H and T_C of each case are shown in Tables 1 and 2. The channel height is determined from the centerline of the first layer of wall molecules on the top and bottom surfaces and the computational domain is divided into bins of approximately σ/10 in size. The schematic sketch of simulation domain is depicted in Fig. 2 in which the periodic boundary conditions are applied in the axial (x) and lateral (z) directions. In order to be able to compare various temperature profiles in the gas medium, all temperature profile are presented in nondimensionalized forms by applying the following equation to all temperature profiles:

$$T(i) = \left(T(i) - 298\right) / \left(\Delta T / 2\right) \tag{3}$$

where $\Delta T = T_H - T_C$ and $T(i)$ is the temperature of the ith bin. In this way, -1 and 1 are assigned to T_C and T_H respectively and the gas temperature profile is scaled between these values accordingly. In order to measure the induced heat flux through the gas domain due to the difference between the temperature of the walls, the following formula is used (Che, Çagin, & Goddard, 2000; Shi, Barisik, & Beskok, 2012):

$$J = \frac{1}{\Omega}\left(\sum_{i=1} v_i e_i + \sum_{i<j} r_{ij}\left(v_i \cdot f_{ij}\right)\right) \tag{4}$$

where J is microscopic heat flux vector, **Ω** is the volume of the system, v_i is velocity of molecule i, e_i is sum of kinetic and potential energy for *ith* molecule and f_{ij} is two-body force between molecules i and j.

Considering the heat flux from Eq. (4) in the perpendicular direction to the walls and the temperature differences between the walls, the Fourier's law is used to determine the effective thermal conductivity of the gas medium (K_{eff}):

$$K_{eff} = J_y \Delta T / H \tag{5}$$

where J_y is the microscopic heat flux in perpendicular direction to the wall.

3. RESULTS

3.1 Determination of the Time Step Size

It was shown that assuming one mean free path in periodic direction and 4 fs for time step size is adequate for calculating the density, velocity and stress profile in nanoconfined flow by the use of SWMD (Barisik & Beskok, 2011a, 2011b; Barisik *et al.*, 2010). Considering the fact that in this study heat transfer is modelled by the use of ITWM, the proper time step is evaluated first to see whether there is any need for smaller time step size or not. Argon at 298 K and ρ=1.896 kg/m^3 is considered in a nanochannel of 5.4 nm in height which mean free path of argon at this state is 54 nm and comparison of that to channel height result in Kn=10 (Barisik & Beskok, 2011a). A temperature difference of 100 K implemented between walls by assuming T_H=348 K and T_C=248 K. The length and the width of the channel are considered as 54 nm and the time step size changes between 4 fs, 2 fs and 1 fs. In all three cases, 20 ns is supposed to reach a steady heat flux through the domain by implementing temperature on each wall after which 80 ns was considered for time averaging. Figure 3(a) depicts the normalized density profile distribution along the height of the channel for various time steps. It is clear that decreasing the time step size have no obvious effect on the accuracy of the result. Normalized temperature variation along channels height is also presented in Fig. 3(b). It is obvious that the density has the same trend as the temperature in respect to the decreasing the time step size. Therefore 4 fs is taken as the time step for all other simulation in this study. This simulation was also repeated for various temperature differences between the walls and all of them show that 4 fs has adequate accuracy for simulation of heat transfer in nano-confined gas but they are not presented here for brevity.

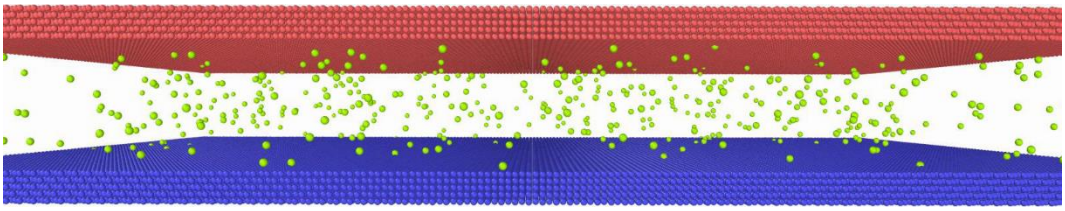

Fig. 2. Three-dimensional snapshot of the simulation domain.

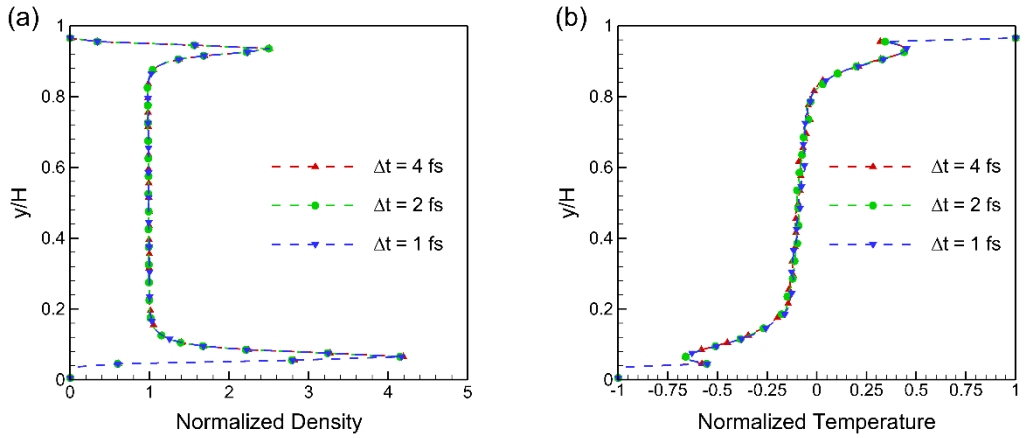

Fig. 3. Normalized density (a) normalized temperature (b) for three different time steps.

4. RESULTS

4.1 Determination of the Time Step Size

It was shown that assuming one mean free path in periodic direction and 4 fs for time step size is adequate for calculating the density, velocity and stress profile in nanoconfined flow by the use of SWMD (Barisik & Beskok, 2011a; 2011b; Barisik *et al.*, 2010). Considering the fact that in this study heat transfer is modelled by the use of ITWM, the proper time step is evaluated first to see whether there is any need for smaller time step size or not. Argon at 298 K and ρ=1.896 kg/m^3 is considered in a nanochannel of 5.4 nm in height which mean free path of argon at this state is 54 nm and comparison of that to channel height result in *Kn*=10 (Barisik & Beskok, 2011a). A temperature difference of 100 K implemented between walls by assuming T_H=348 K and T_C=248 K. The length and the width of the channel are considered as 54 nm and the time step size changes between 4 fs, 2 fs and 1 fs. In all three cases, 20 ns is supposed to reach a steady heat flux through the domain by implementing temperature on each wall after which 80 ns was considered for time averaging. Figure 3(a) depicts the normalized density profile distribution along the height of the channel for various time steps. It is clear that decreasing the time step size have no obvious effect on the accuracy of the result. Normalized temperature variation along channels height is also presented in Fig. 3(b). It is obvious that the density

has the same trend as the temperature in respect to the decreasing the time step size. Therefore 4 fs is taken as the time step for all other simulation in this study. This simulation was also repeated for various temperature differences between the walls and all of them show that 4 fs has adequate accuracy for simulation of heat transfer in nano-confined gas but they are not presented here for brevity.

3.2 Validity of Results

The validity of the results is investigated by comparing the density and velocity profiles with the previous study of argon gas Couette flow (Barisik & Beskok, 2011b). Argon at ρ=1.896 kg/m^3 and *T*=298 K is considered in the domain and the atomistic walls move in opposite directions with a characteristic velocity corresponding to 64 m/s. We let the initial particle distribution to evolve for 1×10^6 time steps (4 ns) to reach an isothermal steady state after which 2×10^6 time steps (8 ns) were performed for time averaging (Barisik & Beskok, 2011b) although longer time averaging is performed to ensure convergence of macroscopic quantity. Three different set of simulations are performed by changing the relaxation time of the applied Nose-Hoover thermostat (Evans & Hoover, 1986). Actually, the relaxation time varies between 0.1, 0.2 and 0.4 ps respectively for the case a, b and c. Figures 4(a) and (b) show the distribution of the normalized density and velocity of the gas near bottom wall respectively.

To further validate the capability of our method in calculating the thermally related properties within the gas medium, the normalized density, and the temperature distribution are compared with Barisik & Beskok (2011a). Argon at ρ=1.896 kg/m3 and T=298 K is considered in a domain of size 54×5.4×54 nm under isothermal conditions. Figures 5(a) and (b) show the distribution of the

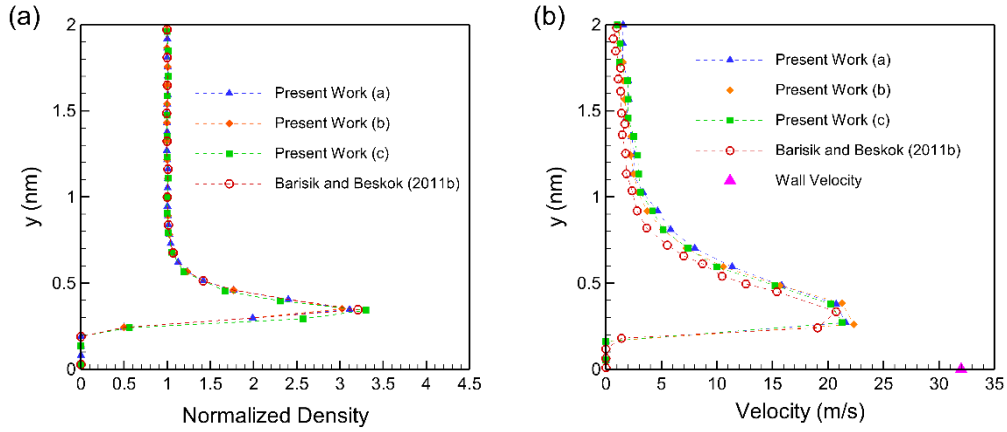

Fig. 4. Normalized density (a) and velocity (b) comparison with Barisik & Beskok (2011b).

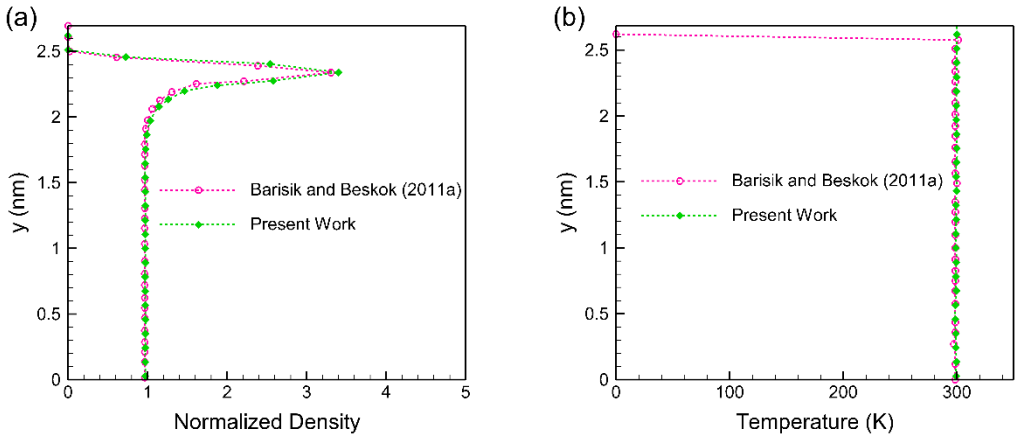

Fig. 5. Normalized density (a) and temperature (b) comparison with Barisik & Beskok (2011a).

normalized density and temperature of the gas in ITWM that is used in this study and the value of the SWMD which was used in Barisik & Beskok (2011a). The result shows that ITWM perfectly captures the SWMD normalized density profile. Moreover, the isothermal nature of the gas domain at 298 K is also captured precisely by the ITWM.

3.3 Two Versus Three Dimensional Models

In contrary to SWMD wall model, in the interactive thermal wall models, all the wall atoms should be simulated during each time steps so the possibility of using 2D simulation instead of 3D ones would reduce the computational cost drastically. So in this part, the temperature and density profiles are compared for both simulations. The simulation details for this set of simulation are depicted in Table 1. It was shown that the specified simulation details for these cases provide the same modified Knudsen number (k=10), so we are able to compare them (Barisik *et al.*, 2010). The temperature difference of 60 K is applied between the channel walls while the initial temperature of the gas was 298 K. The comparison between density and temperature profiles of 2D and 3D simulation is depicted in Figs. 6(a) and (b) respectively.

Figure 6(a) clearly shows that 2D simulation is not able to show the density accumulation that is occurred in the wall force field region in the gas. The reason refers to the fact that in 3D simulation, the effective wall force field on each gas molecules arises from much more wall molecules in comparison with the 2D case (Barisik *et al.*, 2010). Therefore, the smaller wall force field for 2D case leads to the prediction of 1.8 and 1.55 for maximum normalized density near cold and hot wall respectively while in 3D case, the values are 3.36 and 2.52. Figure 6(b) clearly shows that inaccurate prediction of the density distribution in the wall force field region leads to a significant deviation in normalized temperature profile calculation between 2D and 3D case especially in the wall force field region. It should be noted that in the bulk region where the effect of the wall force field is negligible and the gas atoms only interact with each other, 2D simulation predicts the 3D density and temperature profile with good deal of accuracy.

It is inferred from this observation that for a channel above 20 nm height where the wall force field covers a negligible portion of the channel height, the 2D simulation is able to predict the temperature and density profiles in a considerable portion of the channel height accurately.

Table 1 MD simulation details for two and three-dimensional cases

Case	W×H×L (nm)	# Argon atoms	T_H (K)	T_C (K)	n_{ssc}	n_{avr}	K
2D	5.4×600	268	330 K	270 K	1×10^6	10×10^6	10
3D	54×5.4×54	450	330 K	270 K	1×10^6	10×10^6	10

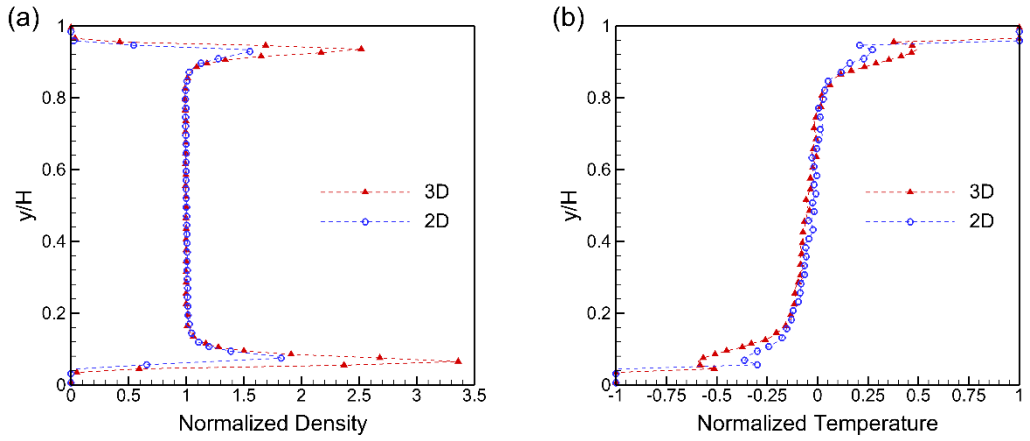

Fig. 6. Normalized density (a) and normalized temperature (b) distributions for 2D and 3D cases.

3.4 Thermal Properties Distribution

In this part, the effect of changing temperature difference between the walls on the variation of different properties such as normalized temperature and density profiles, heat flux, calculated thermal conductivity and thermal resistance of the gas medium is studied. As discussed before, Table 2 implies the specification of the solution parameters and fluid domain. Figure 7(a) shows the distribution of normalized density for three temperature differences along the height of the channel. As is depicted by increasing the temperature differences between the walls, the distribution of argon molecules near each wall has been changed notably. Considering this fact, the behaviour of temperature profile in Fig. 7(b) can be illustrated. Figure 7(b) shows the nondimensionalized temperature variation within the nanochannel height. As the temperature differences increased between the walls, the lower wall temperature decreased and when the argon molecules hit the cold wall, they lose energy so it takes more time for them to escape from the wall force field toward the bulk region. Consequently, the residence time in the wall force field region increases and the gas accumulated near the walls so the density increased. The same behaviour in the opposite direction is also observed for the upper wall. Increasing the temperature differences means higher temperature for the upper wall which leads to increase of energy for the gas molecules which hit this wall. As the consequence, the residence time of gas near wall region is decreased so the density is reduced as it is shown in Fig. 7(b).

It is interesting that based on the temperature difference which is implemented on the walls; the nondimensionalized temperature profile shows different behaviours. The combination of the wall force field and applied temperature differences on the walls not only make changes for distribution of the gas temperature in the near-wall region but also it affects the bulk temperature of the gas. It can be inferred from Figs. 7(a) and (b) that for all temperature differences, the variation of normalized temperature and density due to the combination of wall force field and implemented temperature difference are happening at 1 nm away from each wall. Meanwhile, a linear temperature variation and constant density profile are observed in bulk region of the gas. Figure 8(a) displays the variation of normalized density with changing the temperature differences. It is shown that when the temperature difference varies from 10 K to 200 K, the normalized density changes from 3.2 to 6.5 and this increase in density, changes the magnitude of normalized temperature near bottom wall region from 0.54 to 0.79 as can be observed in Fig. 8(b). It is clear from Fig. 9(a) that while the temperature difference varies from 10 K to 200 K, the maximum value of normalized density near the upper wall changes from 3.2 to 2.1. Figure 9(b) shows that this reduces in density, leads to decrease in maximum value of temperature in wall force field region from 0.57 to 0.35.

Furthermore, it is clearly shown in Figs. 8 and 9 that regardless of the implemented temperature differences between the walls, the maximum value for normalized temperature and density of the gas occur in approximately σ/2 from the first row of wall atoms. This is consistent with the reported data about the distribution of density, stress and velocity in presence of wall force field in nanochannel (Barisik & Beskok, 2011b, 2011a, 2012).

Table 2 MD simulation details for various temperature differences between walls

$T_H - T_C$	T_H (K)	T_C (K)	n_{ssc}	n_{avr}	R_{Total} (μK-m^2/W)	CPU Time (Sec)
10	303	293	30×10^6	120×10^6	26.3	284000
50	323	273	10×10^6	40×10^6	26.61	39500
100	348	248	5×10^6	20×10^6	27.48	19950
150	373	223	3×10^6	10×10^6	28.3	10700
200	398	198	3×10^6	10×10^6	29.85	10700

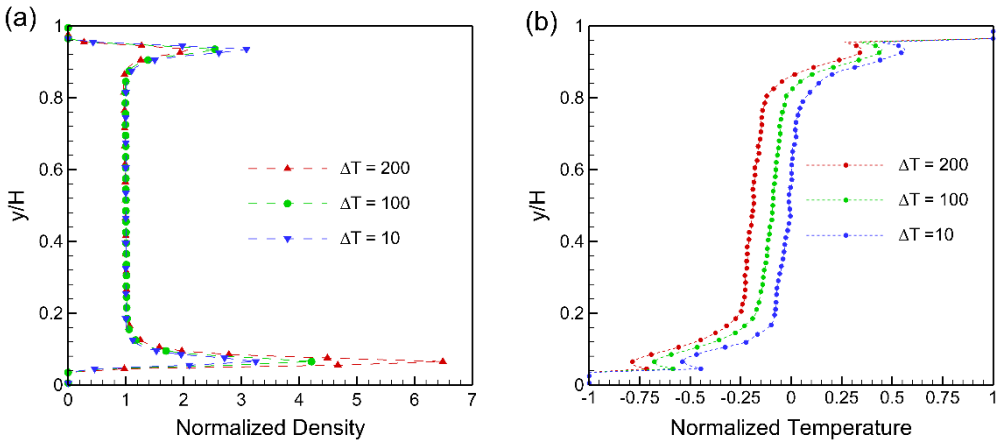

Fig. 7. Normalized density (a) and temperature (b) distributions for temperature differences.

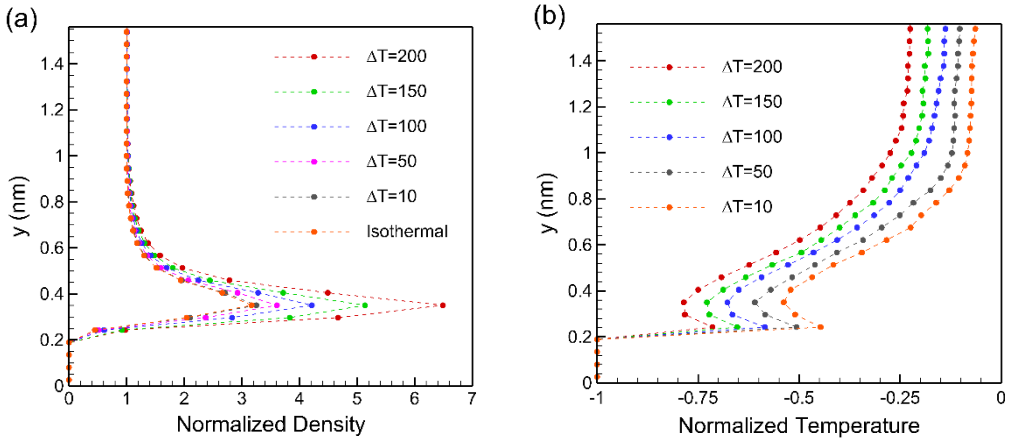

Fig. 8. Variation of normalized density (a) and normalized temperature (b) in 1.5 nm from the lower wall for various temperature differences between the walls.

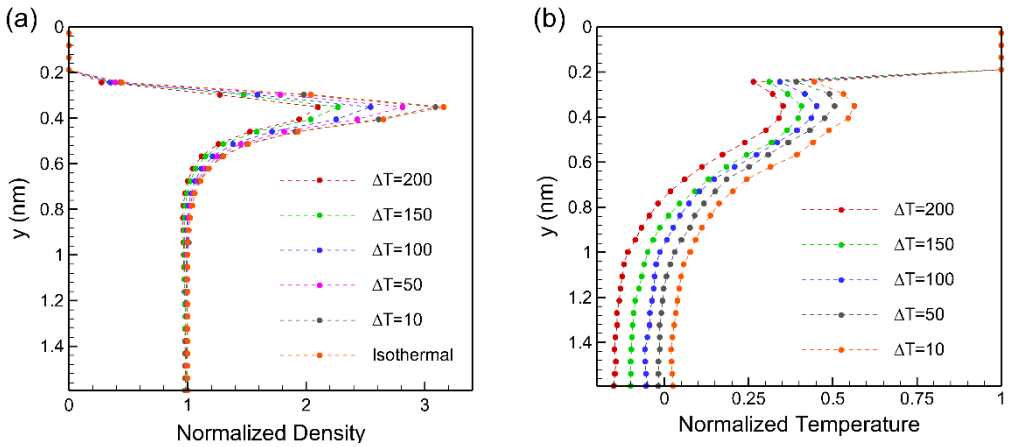

Fig. 9. Variation of normalized density (a) and normalized temperature (b) in 1.5 nm from the upper wall for various temperature differences between the walls.

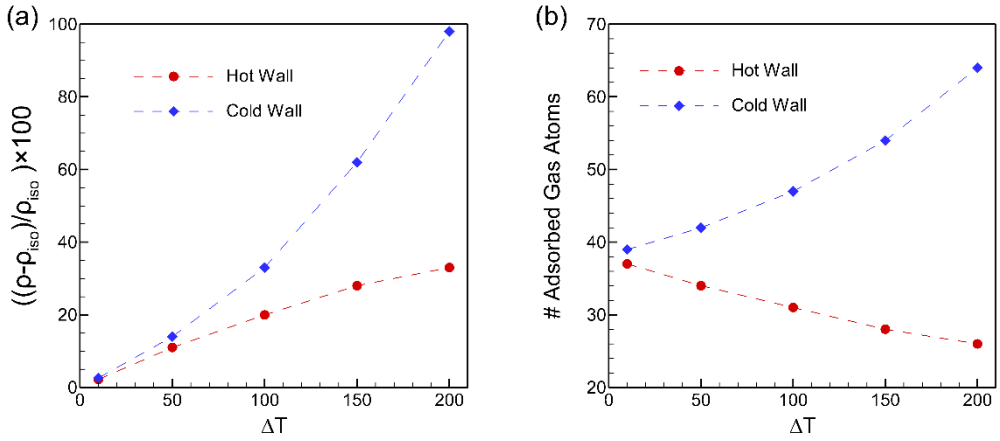

Fig. 10. Variation of maximum density deviation from the isothermal condition (a) and number of absorbed gas atoms on the walls (b) in the near-wall region of warm and cold walls.

Interestingly, the total run time for each case is dependent on the temperature difference between the walls according to Table 2. As the temperature difference between the walls is increased, a stronger heat flux is induced through the gas medium which results in a higher energy transfer from the impinging atom to the walls. It seems that the total run time is directly proportional to the energy transfer to the gas atoms. As the energy transfer rate increases, the required number of timesteps in the averaging part reduces notably which considerably reduces the total run time. It should be noted that all parallel simulations were performed on 80 Intel(R) Xeon(R) CPU E5-2680 v3 @ 2.50GHz cores of a standard Linux cluster with InfiniBand.

The maximum value of normalized density variation in wall force field region from the isothermal simulation versus implemented temperature difference is displayed in Fig. 10(a) for the upper and lower walls. As the deviation of density from the isothermal condition is presented, this figure presents the effect of temperature on density distribution near lower and upper walls. Figure 10(a) clearly shows that while the temperature difference is smaller than 50 K, the variation of density due to temperature differences is about 10% for both walls. When the temperature difference is increased, the deviation of density from the isothermal condition is increased too. As can be seen from this figure for temperature difference in order of 200 K, the normalized density experience a variation in the order of 34% and 103% from the isothermal condition for upper and lower wall respectively that is primarily caused due to implemented temperature. The number of adsorbed gas atoms on each wall is also depicted in Fig. 10(b). It shows the effect of wall temperature on the adsorption of the gas atoms. As the reduction in the number of adsorbed gas atoms for the hot wall varies with a different trend in comparison with the increment near the cold wall, a slight reduction in the bulk gas density is observed.

The maximum and minimum of the gas temperature distribution are depicted in Fig. 11 as the point "e" and "b" respectively. Based on this definition, temperature jump is defined as the absolute difference between the wall temperature and the maximum/minimum of gas temperature near the hot/cold wall and it is shown in Fig 12. In this way, the nondimensionalized temperature jump is a criterion which indicates the relative ability of the wall and gas at the corresponding condition to transfers heat together. It is clear from Fig. 12 that as the temperature differences between the walls increases, the gas temperature gets closer to the cold wall while it deviates more from the hot wall temperature. This is related to the accumulation of the gas molecules near the cold wall that increases the gas-wall molecules collisions which leads to increase the heat transfer capability. Meanwhile, a reduction in the gas density near hot wall happens which results in the reverse effect. Regarding the variation of temperature from 10 K to 200 K between the walls, the corresponding heat flux should be changed for each case. By the use of Eq. (4), this heat flux is calculated and as mentioned before, the thermal conductivity is determined. The calculated heat flux and thermal conductivity are presented in Fig.13.

Figure 13 shows that as it is expected, the heat flux increases by variation of temperature from 10 K to 200 K. Meanwhile, a reduction in the calculated thermal conductivity is also observed. These refer to the change in density distribution near each wall that results from the implemented temperature on the walls as can be found in Fig**.** 10. While for the lower wall the density is increased in the wall force field region, a decrease in the density profile is observed in the wall force field region of the upper wall. It is inferred from Fig. 13 that the cumulative effect of these density changes near the walls leads to a reduction in the calculated thermal conductivity values. Figure 13 is also depicted that the effective thermal conductivity for the implemented temperature difference of 10 K, 50 K and 200 K are 0.198, 0.195 and 0.174 mW/m-k respectively. It clearly shows that meanwhile the difference between the calculated effective thermal conductivity based on 10 K and 50 K is about 1.5%, it increases to 15% when 10 K and 200 K are compared. These observations imply that large

temperature differences cannot be applied for calculating the thermal conductivity of nano-confined gas since it changes the density distribution considerably which result in a reduction in calculated thermal conductivity. It is also observed that the maximum allowed temperature difference for calculating the thermal conductivity is about 50 K which is much faster in comparison with the 10 K according to Table 1.

Considering Fig. 11, distinct regions are observed in which the gas shows different characteristics due to the collision nature. The a-b and e-f regions are the regions that collision between the gas and wall atoms occurs and the gas characteristics are completely affected by these interfacial collisions. These regions are called as "interface region". The b-c and the d-e are the regions where an interplay between the wall force field and gas-gas atom interactions specifies the gas atoms movement and these regions are called "wall force field region".

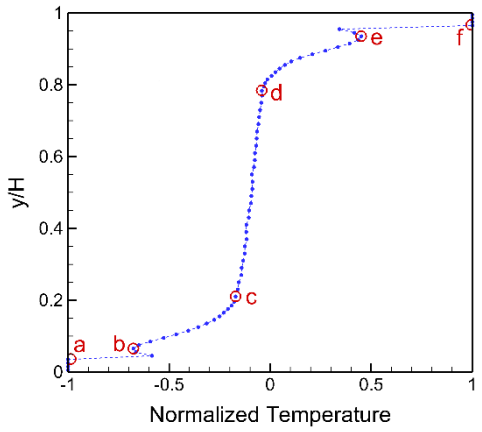

Fig. 11. Decomposition of the temperature profile into different regions.

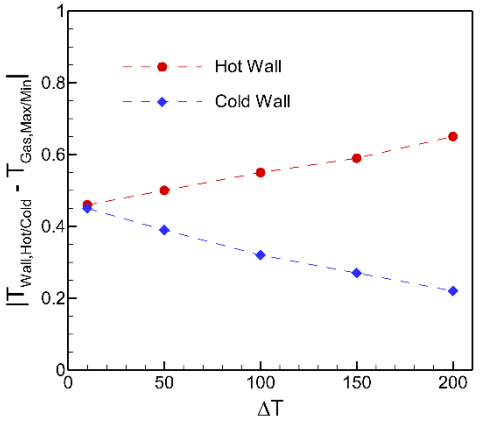

Fig. 12. Variation of the normalized temperature difference between the gas and the walls.

Besides, there is the c-d region in which the wall force field effect is negligible (due to the cut-off radios of the wall atom) and the only effective force in such region is gas-gas atoms interaction which is known as "bulk region". In order to have a better insight through the heat transfer characteristic of the gas medium in each of these different regions, the thermal resistance of each region is calculated based on the $R = \Delta T/J_y$ formula which is applied to each of them separately.

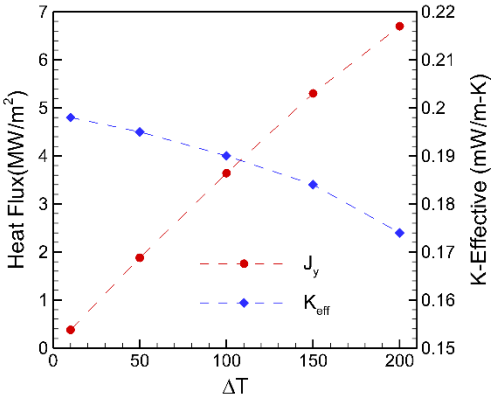

Fig. 13. Variation of heat flux and thermal conductivity through the gas medium for the various temperature difference.

Figure 14(a) shows the variation of the thermal resistance in each layer along the channel height that clearly shows the different nature of each region. It is observed that the minimum thermal resistance occurs in the bulk region where due to rarefied condition, the gas atoms collisions are rare. Furthermore, in the wall force field region where the accumulation of the gas density occurs, the gas atoms collision is intensified and an increase in the thermal resistance is observed. For the interface of the gas medium and the wall atoms, it is shown that the increase in the density near the cold wall leads to a significant reduction in the interfacial resistance. On the other hand, it is observed that reduction in gas density near the hot wall increases the interfacial thermal resistance near the hot wall. Actually, for temperature differences of 10 K, the interfacial thermal resistance near the cold and the hot wall are 6.05 and 5.86 μK-m^2/W respectively while they have changed to 3.28 and 9.7 μK-m^2/W as the temperature differences increased to 200 K.

The total thermal resistance of the gas medium is calculated by the summation of the thermal resistance of all five different regions along the channel height as it is shown in Table 2. It is observed that the total thermal resistance is increased from 26.3 to 29.85 μK-m^2/W as the temperature differences between the walls changes from 10 K to 200 K. It implies that the cumulative effect of density changes near the walls which are observed in Fig. 10, leads to a notable increment of the gas medium total thermal resistance (14% approximately). The calculated total thermal resistance is used for nondimensionalizing the thermal resistance in each region as it is shown in Fig. 14(b). Figure 14(b) clearly reveals the relative importance of each region thermal resistance in comparison with the other ones. As it is shown in this figure, for all temperature differences, the bulk

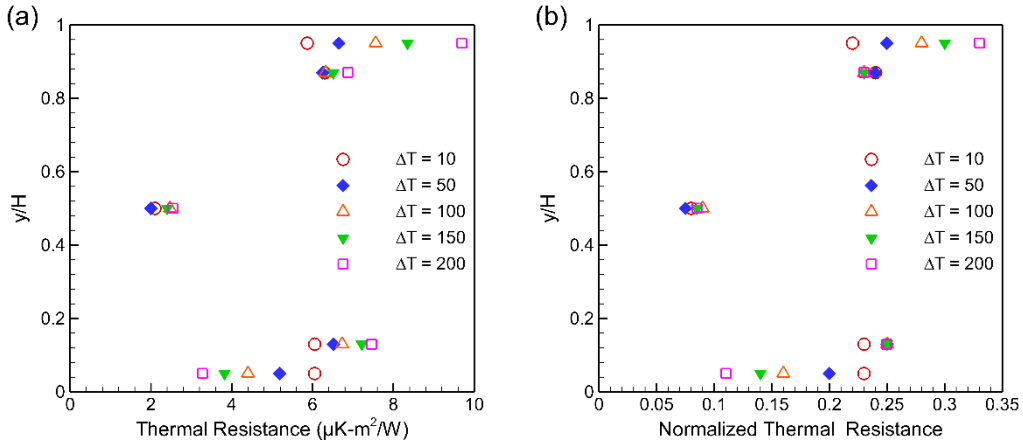

Fig. 14. Variation of (a) thermal resistance and (b) normalized thermal resistance in different gas layer along the channel height.

thermal resistance forms approximately 10% of total thermal resistance while according to Fig. 10, it covers 60% of the channel height. Interestingly, the wall force field regions (b-c and d-e regions) that comprise 35% of the channel height based on Fig. 11, forms approximately 45% of the total thermal resistance regardless of implemented temperature differences between the walls. This higher portion of the thermal resistance refers to an increase in the residence time of the gas atoms which is induced by the presence of the wall force field which leads to more collision between the gas atoms. Finally, it is observed that approximately 45% of total thermal resistance refers to the interfacial thermal resistance between the gas and the solid surfaces (a-b and e-f regions in Fig. 11). This implies that by choosing an appropriate martial for the walls that have smaller interface thermal resistance with the gas atoms, the total thermal resistance could reduce notably which will inevitably lead to higher heat transfer rate. Furthermore, it is observed that while the thermal resistance of the bulk and wall force field regions are independent of the implemented temperature differences, the interfacial thermal resistance between the gas and the walls strongly depends on the wall temperature.

5. CONCLUSIONS

Heat transfer characteristics of nano-confined static argon gas are investigated while the gas is rarefied (k=10) and the wall force field covers a considerable channel height. The significance of the wall force field in the vicinity of about 1 nm from each wall on the density and temperature distribution is observed. The following conclusions can be drawn from the results:

1. While the 2-D simulation underestimates the density and temperature values in the wall force field regions, it still predicts the density and temperature distribution of the gas with good accuracy in comparison with the 3D model with a remarkably lower computational cost. Therefore, for any future research where the main goal is to study the density and temperature profiles in the bulk region of nanoconfined gas media, the 2-D model provides adequate accuracy with substantially lower computational time. However, when precise resolution near the walls is required, the 3-D model should be applied.
2. Regardless of implemented temperature differences between the walls, the maximum density and temperature occurs at a distance of σ/2 from the walls.
3. The combination of the wall force field and implemented temperature differences determines the distribution of the gas atoms in the channel. This leads to the fact that for various temperature differences between the walls, different normalized temperature profiles are observed in the gas medium all over of the channel height.
4. As the upper wall becomes hotter, the energy of impinging gas molecules is increased which leads to a reduction of the gas atoms residence time. Furthermore, by decreasing the temperature of the lower wall, the residence time increases notably. Future research shall be conducted to quantify the residence time of gas atoms in the wall force field region and the effect of wall temperature on the reduction and increment of the residence time.
5. The variation of effective thermal conductivity by changing the wall temperature differences reveals that for calculating the effective thermal conductivity based on the nano-confined gas heat conduction, the implemented temperature differences between the channel walls should not exceed 50 K.
6. Based on the thermal resistance analysis, five different regions are observed along the channel height where the gas transport characteristics are different.
7. While the bulk region occupies 60% of the channel height, it only forms approximately

10% of the total thermal resistance. Meanwhile, the wall force field regions occupy approximately 35% of the channel height and form 45% of the total thermal resistance. This implies that nearly 45% of total thermal resistance refers to the interfacial thermal resistance. Due to this considerable portion, changing the wall material shall notably vary induced heat flux through the domain. Therefore, future research shall be focused on the use of various wall materials to increase or decrease the interfacial thermal resistance based on the desired application.

8. As the bulk and wall force field regions thermal resistance are approximately independent of the implemented temperature on the walls, the interfacial thermal resistance near the cold and the hot wall are strongly dependent to the wall temperature.

9. Since the gas atoms distribution along the channel height is a function of both the temperature differences between the walls and the temperature of each wall, the number of gas atoms in each case should be tuned properly to have the desired gas density in the middle of the channel.

10. Considering the significant variation of the absorbed gas atom number on the walls with the temperature, the combined effect of changing the wall-gas atom interaction strength and wall temperature on the number of absorbed gas atoms, shall be an interesting subject for future research.

REFERENCES

Allen, M. P., D. J. Tildesley and J. R. Banavar (1989). Computer Simulation of Liquids. *Physics Today* 42(3), 105-106.

Amani, A., S. M. H. Karimian and M. Seyednia (2017). A molecular dynamics simulation on the effect of different parameters on thermal resistance of graphene-argon interface. *Molecular Simulation* 43(4), 276-283.

Asproulis, N. and D. Drikakis (2010). Boundary slip dependency on surface stiffness. *Physical Review E - Statistical, Nonlinear, and Soft Matter Physics* 81(6), 1-5.

Barisik, M. and A. Beskok (2011a). Equilibrium molecular dynamics studies on nanoscale-confined fluids. *Microfluidics and Nanofluidics* 11(3), 269-282.

Barisik, M. and A. Beskok (2011b). Molecular dynamics simulations of shear-driven gas flows in nano-channels. *Microfluidics and Nanofluidics* 11(5), 611-622.

Barisik, M. and A. Beskok (2012). Surface-gas interaction effects on nanoscale gas flows. *Microfluidics and Nanofluidics* 13(5), 789-798.

Barisik, M. and A. Beskok (2014). Scale effects in gas nano flows. *Physics of Fluids* 26(5), 052003.

Barisik, M. and A. Beskok (2015). Molecular free paths in nanoscale gas flows. *Microfluidics and Nanofluidics* 18(5-6), 1365-1371.

Barisik, M. and A. Beskok (2016). "Law of the nano-wall" in nano-channel gas flows. *Microfluidics and Nanofluidics* 20(3), 1-9.

Barisik, M., B. Kim and A. Beskok (2010). Smart wall model for molecular dynamics simulations of nanoscale gas flows. *Communications in Computational Physics* 7(5), 977-993.

Cao, B. Y., J. Sun, M. Chen and Z. Y. Guo (2009). Molecular momentum transport at fluid-solid interfaces in MEMS/NEMS: A review, 10 International Journal of Molecular Sciences § (2009). Multidisciplinary Digital Publishing Institute (MDPI).

Che, J., T. Çagin, T. and W. A. Goddard (2000). Thermal conductivity of carbon nanotubes. *Nanotechnology* 11(2), 65-69.

Evans, D. J. and W. G. Hoover (1986). Flows Far From Equilibrium Via Molecular Dynamics. *Annual Review of Fluid Mechanics* 18(1), 243-264.

Faraji, F. and A. Rajabpour (2017). Fluid heating in a nano-scale Poiseuille flow: A non-equilibrium molecular dynamics study. *Current Applied Physics* 17(12), 1646-1654.

Fu, T. and Q. Wang (2018). Effect of nanostructure on heat transfer between fluid and copper plate: a molecular dynamics simulation study. *Molecular Simulation* 1–6.

Ge, S., Y. Gu and M. Chen (2015). A molecular dynamics simulation on the convective heat transfer in nanochannels. *Molecular Physics* 113(7), 703-710.

Ghorbanian, J. and J. Beskok (2017). Temperature profiles and heat fluxes observed in molecular dynamics simulations of force-driven liquid flows. *Physical Chemistry Chemical Physics* 19(16), 10317-10325.

Jepps, O. G., S. K. Bhatia and D. J. Searles (2004). Modeling molecular transport in slit pores. *Journal of Chemical Physics* 120(11), 5396-5406.

Kammara, K. K., G. Malaikannan and R. Kumar (2016). Molecular Dynamics Study of Gas–Surface Interactions in a Force-Driven Flow of Argon through a Rectangular Nanochannel. *Nanoscale and Microscale Thermophysical Engineering* 20(2), 121–136.

Kim, B. H., A. Beskok and T. Cagin (2008). Thermal interactions in nanoscale fluid flow: Molecular dynamics simulations with solid-liquid interfaces. *Microfluidics and Nanofluidics* 5(4), 551-559.

Liu, B., S. Yu, M. Zhang, L. Gonzaga, H. Li, J. Liu and Y. Ma (2007). Air-Bearing Design Towards Highly Stable Head – Disk Interface at Ultralow Flying Height 43(2), 715-720.

Markvoort, A. J., P. A. J. Hilbers and S. V. Nedea (2005). Molecular dynamics study of the influence of wall-gas interactions on heat flow in nanochannels. *Physical Review E* 71(6), 066702.

Matthes, L. M., B. Knigge and F. E. Talke (2014). Head-disk proximity sensing using contact sensors in hard disk drives. *IEEE Transactions on Magnetics* 50(11), 1–4.

Morciano, M., M. Fasano, A. Nold, C. Braga, P. Yatsyshin, D. N. Sibley, B. D. Goddard, E. Chiavazzo, P. Asinari, S. Kalliadasis (2017). Nonequilibrium molecular dynamics simulations of nanoconfined fluids at solid-liquid interfaces. *The Journal of Chemical Physics* 146(24), 244507.

Myo, K. S., W. Zhou, S. Yu and W. Hua (2011). Direct Monte Carlo simulation of air bearing effects in heat-assisted magnetic recording. In *Microsystem Technologies* 17, 903–909.

Plimpton, S. (1995). Fast Parallel Algorithms for Short-Range Molecular Dynamics. *Journal of Computational Physics*, *117*(1), 1–19.

Pop, E. (2010, March 5). Energy dissipation and transport in nanoscale devices. *Nano Research*. Tsinghua Press.

Prabha, S. K. and S. P. Sathian (2013). Calculation of thermo-physical properties of Poiseuille flow in a nano-channel. *International Journal of Heat and Mass Transfer* 58(1-2), 217-223.

Qian, L., C. Tu, F. Bao and Y. Zhang (2016). Virtual-Wall Model for Molecular Dynamics Simulation. *Molecules* 21(12), 1678.

Rebay, M., Y. Kabar and S. Kakaç (2016). *Microscale and Nanoscale Heat Transfer: Analysis, Design, and Application*. *CRC Press*. CRC Press.

Schaaf, S. A. and P. A.Chambr. (1961). *Flow of Rarefied Gases*. *Princeton University Press*. Princeton University Press.

Shi, Z., M. Barisik and A. Beskok (2012). Molecular dynamics modeling of thermal resistance at argon-graphite and argon-silver interfaces. *International Journal of Thermal Sciences* 59, 29–37.

Soong, C. Y., T. H. Yen and P. Y. Tzeng (2007). Molecular dynamics simulation of nanochannel flows with effects of wall lattice-fluid interactions. *Physical Review E*, 76(3), 036303.

Volz, S. and R. Carminati (2007). *Microscale and nanoscale heat transfer*. *Microscale and Nanoscale Heat Transfer*. Boca Raton FL: CRC Press.

Wang, X., P. Cheng and X. Quan (2016). Molecular dynamics simulations of thermal boundary resistances in a liquid between two solid walls separated by a nano gap. *International Communications in Heat and Mass Transfer* 77, 183-189.

Yasuoka, H., M. Kaneda and K. Suga (2016). Wall-Adjacent Velocity Profiles of Nano-scale Gas Flows. *Journal of Statistical Physics* 165(5), 907-919.

Zhou, W., B. Liu, S. Yu and W. Hua (2010). Numerical simulations of accommodation coefficient effects at the head-disk interface. *Japanese Journal of Applied Physics* 49(9 PART 1), 095206.

Zhou, W., S. Yu, W. Hua and K. S. Myo (2013). A modified slip model for gas lubrication at nanoscale head-disk interface. *Proceedings of the Institution of Mechanical Engineers, Part J: Journal of Engineering Tribology* 227(12), 1367-1375.